


Broadband optical nonreciprocity via nonreciprocal band structureNing Hu,¹ Zhi-Xiang Tang,¹ and Xun-Wei Xu ^{1,2,*}¹*Department of Physics and Synergetic Innovation Center for Quantum Effects and Applications, Key Laboratory of Low-Dimensional Quantum Structures and Quantum Control of Ministry of Education, Key Laboratory for Matter Microstructure and Function of Hunan Province, Hunan Normal University, Changsha 410081, China*²*Institute of Interdisciplinary Studies, Hunan Normal University, Changsha, 410081, China*

(Received 27 September 2023; accepted 4 December 2023; published 22 December 2023)

As a promising approach for optical nonreciprocity without magnetic materials, optomechanically induced nonreciprocity has great potential for all-optical controllable isolators and circulators on integrated photonic chips. However, as a very important issue in practical applications, the bandwidth for nonreciprocal transmission with high isolation has not been fully investigated yet. In this study we first review the nonreciprocity in a Brillouin optomechanical system with single cavity mode and point out the challenge in achieving broad bandwidth with high isolation. To overcome this challenge, we propose a one-dimensional optomechanical array to realize broadband optical nonreciprocity via nonreciprocal band structure. We exploit nonreciprocal band structure induced by the stimulated Brillouin scattering with directional optical pumping and show that it is possible to demonstrate optical nonreciprocity with both broad bandwidth and high isolation. Such optomechanical lattices with nonreciprocal band structure, offer an avenue to explore nonreciprocal collective effects of both photons and phonons in different frequency regimes.

DOI: [10.1103/PhysRevA.108.063516](https://doi.org/10.1103/PhysRevA.108.063516)**I. INTRODUCTION**

Cavity optomechanics for the optical and mechanical modes coupled through parameters interaction (for review, see Ref. [1]) is a rapidly developing field and has wide applications ranging from gravitational wave detections [2] to modern quantum technologies [3]. Recent studies [4] indicate that the optomechanical system is an elegant candidate for implementing optical nonreciprocity without magnetic materials. Based on the optomechanical interactions, many nonreciprocal devices, such as isolators and circulators, are proposed theoretically via various of mechanisms, including asymmetric optomechanical nonlinear interaction [5–8], directional enhanced optomechanical interaction in whispering-gallery-mode (WGM) microresonators [9–12], synthetic magnetism for a closed loop of optical and mechanical modes with nontrivial topological phases [13–29], and dynamical encircling of the exceptional point [30,31]. As a versatile platform, nonreciprocity has been realized in various optomechanical systems working in different frequency domains, ranging from optical regime with a silica microsphere or microtoroid [32–38], a silicon nitride membrane placed inside a high-finesse optical cavity [39–41], and a silicon optomechanical crystal circuit [42–44], to the microwave regime implemented in superconducting microwave circuits [45–49].

As an essential parameter, the isolation of nonreciprocity has been seriously studied from both the theoretical and experimental aspects. However, as another important parameter, the bandwidth of nonreciprocity has attracted much less

attention in past studies. It has been shown that the bandwidth of the optomechanically induced nonreciprocity is ultimately limited by the optical linewidths [9,35]. So far, how to break the bandwidth limit of nonreciprocity is still an open question. To answer this question, we propose to demonstrate optomechanical nonreciprocity in an optomechanical array with nonreciprocal band structure that simultaneously favors broad bandwidth and high reverse isolation.

In a very recent work [50], nonreciprocal single-photon band structure was proposed in a one-dimensional (1D) coupled-resonator optical waveguide that chirally couples to an array of two-level quantum emitters. Inspired by this work [50] and the rapid growth of topological optomechanical lattices [51,52], here we propose to realize optomechanical nonreciprocity with high reverse isolation and broad bandwidth via nonreciprocal band structure in a Brillouin optomechanical array. The nonreciprocal band structure is generated by the stimulated Brillouin scattering between the optical and mechanical whispering-gallery modes (WGMs) circulating along the equatorial surface with the control laser maintained in one direction, which is obviously different from the nonreciprocal band structure based on chirally coupling to two-level quantum emitters [50]. Our work is also different from the nonreciprocal phonon transport that was proposed in an array of optomechanical cavities with time-reversal symmetry broken by the position-dependent phase (synthetic magnetic field) [23] or the interplay of photonic spin-orbit coupling [53,54].

This rest of the paper is organized as follows. In Sec. II, we give a brief review on the optical nonreciprocity based on stimulated Brillouin scattering in a WGM optomechanical system, and elaborate the challenge we face in achieving

*xwxu@hunnu.edu.cn

optical nonreciprocity with both broad bandwidth and high isolation in a single cavity. We propose to realize nonreciprocal band structure in a Brillouin optomechanical array in Sec. III. In Sec. IV, we demonstrate the optomechanical nonreciprocity with high reverse isolation and broad bandwidth via the nonreciprocal band structure, show the advantageous of optomechanical nonreciprocity via the nonreciprocal band structure to the nonreciprocity in the Brillouin optomechanical system with single cavity, and discuss the effect of the backscattering on the nonreciprocity. Finally, we summarize the results in Sec. V.

II. PHOTON-PHONON-INTERACTION-INDUCED NONRECIPROcity

We start by reviewing optical nonreciprocity induced by photon-phonon interactions in a microresonator supporting pairs of degenerate clockwise (CW) and counterclockwise (CCW) WGMs, which has been realized by several different experimental groups based on Brillouin scattering [32,33] or optomechanical interaction [34–37]. We will discuss the bandwidth for nonreciprocal transport between different ports with high isolation and show the challenge we face in achieving the optical nonreciprocity with both broad bandwidth and high isolation in a single cavity.

As a specific example, we consider a Brillouin optomechanical system that consists of a microcavity supporting both optical and mechanical WGMs traveling along the surface, and the optical modes are evanescently coupled with two tapered fibres, as illustrated schematically in Fig. 1(a). The optomechanical system based on forward Brillouin scattering can be described with the Hamiltonian

$$\begin{aligned} H_{\text{Bom}} = & \sum_{\sigma=\text{cw,ccw}} (\omega_0 a_\sigma^\dagger a_\sigma + \omega_c c_\sigma^\dagger c_\sigma + \omega_d d_\sigma^\dagger d_\sigma) \\ & + \sum_{\sigma=\text{cw,ccw}} g_b (d_\sigma a_\sigma^\dagger c_\sigma + d_\sigma^\dagger a_\sigma c_\sigma^\dagger) \\ & + (\Omega e^{-i\omega_p t} d_{\text{cw}}^\dagger + \Omega^* e^{i\omega_p t} d_{\text{cw}}), \end{aligned} \quad (1)$$

where a_σ and d_σ are two optical modes coupled through Brillouin scattering mediated by the traveling acoustic wave c_σ in the same direction. Here (ω_0, k_0) and (ω_d, k_d) are the energies and momenta of the optical modes a_σ and d_σ , and (ω_c, k_c) are the energy and momentum of the travelling acoustic mode. To observe the forward Brillouin scattering effect, the energies and momenta of these three modes must satisfy the energy and momentum conservations $\omega_c = \omega_0 - \omega_d$ and $k_c = k_0 - k_d$ simultaneously. To enhance the single-photon Brillouin coupling rate g_b , a strong control laser (Ω and ω_p) is input from Port 1. For simplicity, we assume that the frequencies of the modes satisfy the resonant conditions $\omega_p = \omega_d = \omega_0 - \omega_c$ [Fig. 1(a)].

In a rotating frame defined by the unitary transformation operator $R_1(t) = \exp(-iH_0 t)$ with $H_0 = \sum_{\sigma=\text{cw,ccw}} (\omega_0 a_\sigma^\dagger a_\sigma + \omega_c c_\sigma^\dagger c_\sigma + \omega_d d_\sigma^\dagger d_\sigma)$, the Hamiltonian (1) becomes

$$H'_{\text{Bom}} = \sum_{\sigma=\text{cw,ccw}} g_b (d_\sigma a_\sigma^\dagger c_\sigma + d_\sigma^\dagger a_\sigma c_\sigma^\dagger) + (\Omega d_{\text{cw}}^\dagger + \Omega^* d_{\text{cw}}). \quad (2)$$

For a very strong control laser pumping to mode d_{cw} , we can treat the operator of the mode d_{cw} as a sum of its classical mean value and quantum fluctuation operator $\langle d_{\text{cw}} \rangle + d_{\text{cw}}$, where $\langle d_{\text{cw}} \rangle = -i\Omega/\kappa_d$ and κ_d is the coupling strength between the optical mode and fibers. Then, we obtain the linearized photon-phonon interaction as

$$H_{\text{bom}} \approx g a_{\text{cw}}^\dagger c_{\text{cw}} + g^* a_{\text{cw}} c_{\text{cw}}^\dagger, \quad (3)$$

where $g \equiv g_b \langle d_{\text{cw}} \rangle$ is enhanced by the strong control laser with $\langle d_{\text{cw}} \rangle \gg 1$, and the weak nonlinear terms $\sum_{\sigma=\text{cw,ccw}} g_b (d_\sigma a_\sigma^\dagger c_\sigma + \text{H.c.})$ are ignored. Though the nonlinear interaction may induce quantum correlations [55], here this effect can be ignored for weak nonlinear interaction ($g_b \ll \kappa_d$) under the conditions that both the power of the probe laser and the amplitude of the acoustic wave are very weak in the following. Without loss of generality, we take g as a positive-real number in the following. We note that this strong driving-enhanced beam-splitter-type photon-phonon interaction has also been realized in the optomechanical systems for the WGM optical modes coupling with the breathing mechanical mode [34–37]. So the results in the following are also applicable to the other WGM optomechanical systems. The transmission spectra of the probe laser input from different port can be obtained analytically by means of the Fourier transformation method. The quantum Langevin equations (QLEs) are given by

$$\frac{d}{dt} a_{\text{cw}} = -\kappa_a a_{\text{cw}} - ig c_{\text{cw}} + \sqrt{\kappa_a} a_{1,\text{in}} + \sqrt{\kappa_a} a_{4,\text{in}}, \quad (4)$$

$$\frac{d}{dt} c_{\text{cw}} = -\kappa_c c_{\text{cw}} - ig a_{\text{cw}} + \sqrt{2\kappa_c} c_{\text{cw},\text{in}}, \quad (5)$$

$$\frac{d}{dt} a_{\text{ccw}} = -\kappa_a a_{\text{ccw}} + \sqrt{\kappa_a} a_{2,\text{in}} + \sqrt{\kappa_a} a_{3,\text{in}}, \quad (6)$$

where the optical modes a_{cw} and a_{ccw} are coupled to both of the fibers with strength κ_a , and $a_{j,\text{in}}$ is the field input from Port j ; κ_c is the acoustic damping rate and $c_{\text{cw},\text{in}}$ is the field input into the acoustic mode. The QLEs can be solved in the frequency domain by introducing the Fourier transform for an operator o as

$$\tilde{o}(\omega) = \frac{1}{\sqrt{2\pi}} \int_{-\infty}^{+\infty} o(t) e^{i\omega t} dt. \quad (7)$$

Based on the standard input-output theory [56]

$$\tilde{a}_{1,\text{out}}(\omega) + \tilde{a}_{2,\text{in}}(\omega) = \sqrt{\kappa_a} \tilde{a}_{\text{ccw}}(\omega), \quad (8)$$

$$\tilde{a}_{2,\text{out}}(\omega) + \tilde{a}_{1,\text{in}}(\omega) = \sqrt{\kappa_a} \tilde{a}_{\text{cw}}(\omega), \quad (9)$$

$$\tilde{a}_{3,\text{out}}(\omega) + \tilde{a}_{4,\text{in}}(\omega) = \sqrt{\kappa_a} \tilde{a}_{\text{cw}}(\omega), \quad (10)$$

we obtain the expressions of the output fields as

$$\tilde{a}_{1,\text{out}}(\omega) = S_{12}(\omega) \tilde{a}_{2,\text{in}}(\omega) + S_{13}(\omega) \tilde{a}_{3,\text{in}}(\omega), \quad (11)$$

$$\begin{aligned} \tilde{a}_{2,\text{out}}(\omega) = & S_{21}(\omega) \tilde{a}_{1,\text{in}}(\omega) + S_{24}(\omega) \tilde{a}_{4,\text{in}}(\omega) \\ & + S_{2c}(\omega) \tilde{c}_{\text{cw},\text{in}}(\omega), \end{aligned} \quad (12)$$

$$\begin{aligned} \tilde{a}_{3,\text{out}}(\omega) = & S_{31}(\omega) \tilde{a}_{1,\text{in}}(\omega) + S_{34}(\omega) \tilde{a}_{4,\text{in}}(\omega) \\ & + S_{3c}(\omega) \tilde{c}_{\text{cw},\text{in}}(\omega), \end{aligned} \quad (13)$$

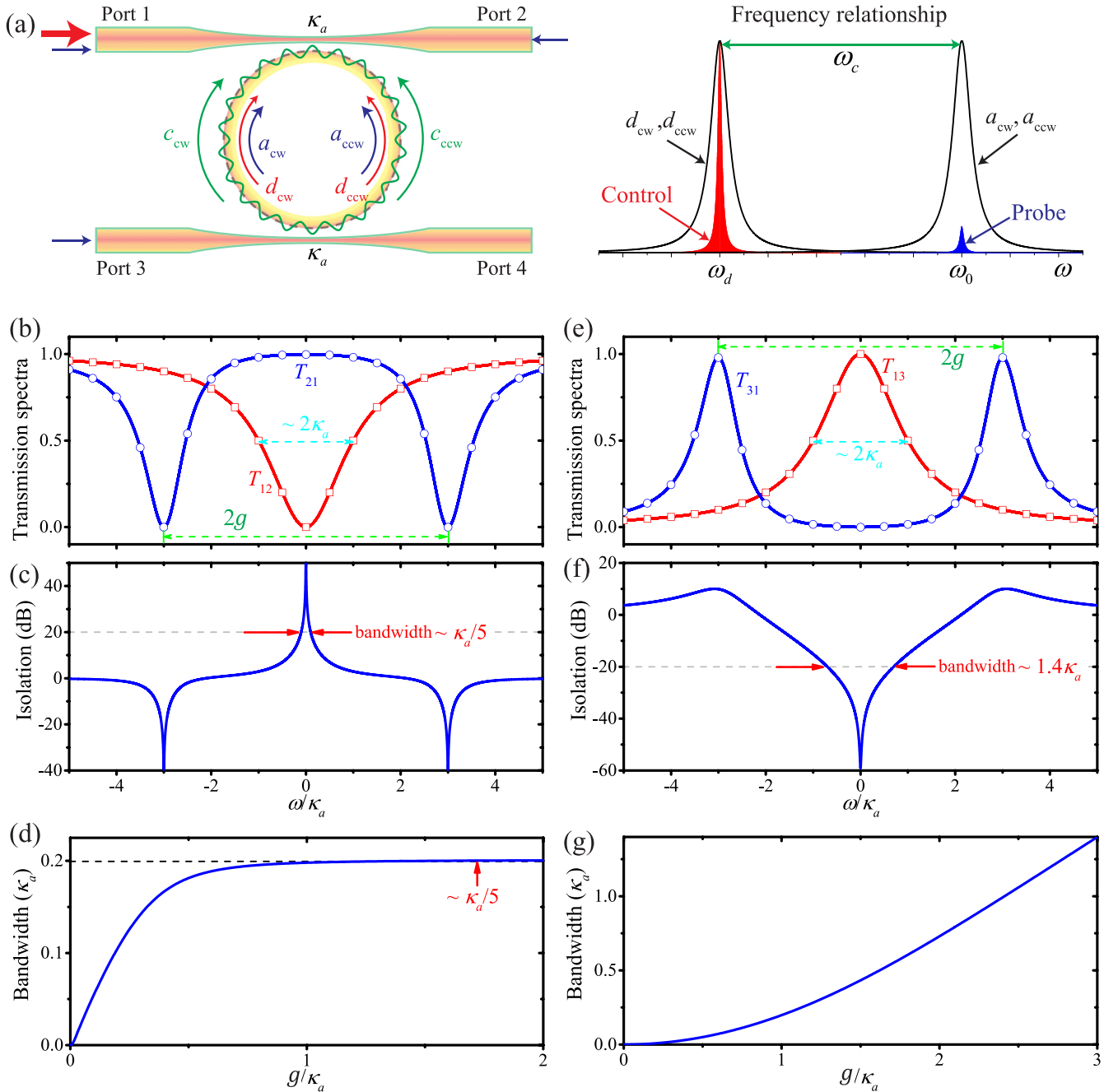


FIG. 1. (a) Schematic illustration of the forward Brillouin optomechanical interaction and the frequency relationship under triple resonance $\omega_0 = \omega_d + \omega_c$. (b) [(e)] The transmission spectra (T_{12} and T_{21}) [T_{13} and T_{31}] and (c) [(f)] the isolation $10 \log_{10}(T_{21}/T_{12})$ [$10 \log_{10}(T_{31}/T_{13})$] for $g = 3\kappa_a$. (d) [(g)] The bandwidth for the 20 dB isolation ($T_{21}/T_{12} = 100$) [$T_{31}/T_{13} = 0.01$] versus coupling g/κ_a . Here we set $\kappa_c = \kappa_a/100$.

where

$$S_{12}(\omega) = \frac{\kappa_a}{\kappa_a - i\omega} - 1, \quad (14)$$

$$S_{21}(\omega) = S_{34}(\omega) = \frac{(\kappa_c - i\omega)\kappa_a}{(\kappa_a - i\omega)(\kappa_c - i\omega) + g^2} - 1, \quad (15)$$

$$S_{13}(\omega) = \frac{\kappa_a}{\kappa_a - i\omega}, \quad (16)$$

$$S_{31}(\omega) = S_{24}(\omega) = \frac{(\kappa_c - i\omega)\kappa_a}{(\kappa_a - i\omega)(\kappa_c - i\omega) + g^2}, \quad (17)$$

$$S_{2c}(\omega) = S_{3c}(\omega) = \frac{-ig\sqrt{2\kappa_a\kappa_c}}{(\kappa_a - i\omega)(\kappa_c - i\omega) + g^2}, \quad (18)$$

are the scattering coefficients. The transmission spectra are defined by

$$T_{ij} = |S_{ij}(\omega)|^2 \quad (19)$$

for photons transporting from Port j to i .

The transmission spectra and the corresponding isolation between Ports 1 and 2 are shown in Figs. 1(b) and 1(c). We

can see that the photons transport unidirectionally from Ports 1 to 2 around the frequency $\omega = 0$, or from Ports 2 to 1 around the frequencies $\omega = \pm g$. Such Brillouin-scattering-induced nonreciprocity was realized first in 2015 [32,33]. It is worth emphasizing that the bandwidth for nonreciprocity with high isolation is very narrow. We note that the bandwidth for nonreciprocity depends on the optomechanical coupling strength g . To clarify this point further, we show the bandwidth for 20 dB isolation versus g in Fig. 1(d). It shows that the bandwidth for 20 dB isolation increases with g in the weak coupling regime ($g < \kappa_a$), and then reaches the maximal value about $\kappa_a/5$ in the strong coupling regime ($g > \kappa_a$). The bandwidth with high isolation is one of the most important parameters for nonreciprocal devices in practical applications. How to increase the bandwidth with high isolation still needs more research.

Optical nonreciprocity can also be realized between Ports 1 and 3. According to the transmission spectra and the corresponding isolation shown in Figs. 1(e) and 1(f), the photons transport unidirectionally from Ports 3 to 1 around the frequency $\omega = 0$, or from Ports 1 to 3 around the frequencies $\omega = \pm g$. As shown in Fig. 1(g), the bandwidth for -20 dB isolation increases monotonously with coupling strength g , and most importantly, the value of bandwidth is not saturated in the strong coupling regime. So we can obtain a much broader bandwidth for high isolation between Ports 1 and 3. How to get a broader bandwidth with a higher isolation is the main issues discussed in this paper. We will show that both the bandwidth and isolation for optical nonreciprocity can be improved in a one-dimensional (1D) optomechanical array via nonreciprocal band structure.

III. NONRECIPROCAL BAND STRUCTURE

We propose a 1D optomechanical array with N unit cells as shown in Fig. 2(a), where the unit cell is consisting of a Brillouin optomechanical system coupled to a WGM microresonator. It is worth mentioning that optomechanical arrays were realized in coupled optomechanical double-disk oscillators [57], optomechanical crystals [51], and superconducting circuit optomechanics [52]. In the rotating frame defined by the unitary transformation operator $R_N(t) = \exp(-iH_N t)$ with $H_N = \sum_{\sigma=cw,ccw} \sum_{j=1}^N (\omega_0 a_\sigma^\dagger a_\sigma + \omega_0 b_\sigma^\dagger b_\sigma + \omega_c c_\sigma^\dagger c_\sigma + \omega_d d_\sigma^\dagger d_\sigma)$, the system can be described by the total Hamiltonian

$$H_{\text{tot}} = H_{1 \rightarrow 3}^{(0)} + H_{3 \rightarrow 1}^{(0)} + H_{\text{BS}}^{(0)}, \quad (20)$$

where $H_{1 \rightarrow 3}^{(0)}$ is the Hamiltonian for photons transport from Ports 1 to 3,

$$H_{1 \rightarrow 3}^{(0)} = \sum_{j=1}^N (g_j d_{j,cw}^\dagger a_{j,cw} c_{j,cw}^\dagger + \Omega_j d_{j,cw}^\dagger + v a_{j,cw} b_{j,cw}^\dagger) + \sum_{j=1}^{N-1} v a_{j+1,cw} b_{j,cw}^\dagger + \text{H.c.}, \quad (21)$$

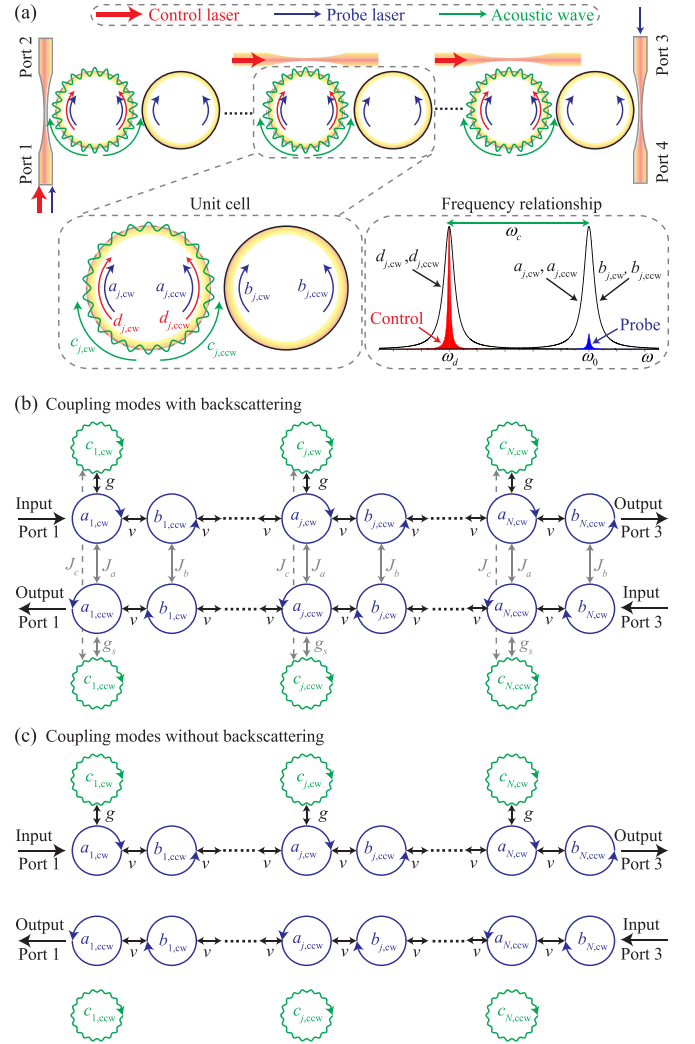


FIG. 2. (a) Schematic of a 1D Brillouin optomechanical array containing N unit cells and the input-output waveguides. (b) Geometric structure of the lattice with the backscattering effect taken account $J_\eta \neq 0$. (c) Geometric structure of the lattice without taking account of the backscattering effect $J_\eta = 0$.

$H_{3 \rightarrow 1}^{(0)}$ is the one for photons transport in the reverse direction, i.e., from Ports 3 to 1,

$$H_{3 \rightarrow 1}^{(0)} = \sum_{j=1}^N (g_j d_{j,ccw}^\dagger a_{j,ccw} c_{j,ccw}^\dagger + v a_{j,ccw} b_{j,cw}^\dagger) + \sum_{j=1}^{N-1} v a_{j+1,ccw} b_{j,cw}^\dagger + \text{H.c.}, \quad (22)$$

and

$$H_{\text{BS}}^{(0)} = \sum_{j=1}^N \sum_{\eta=a,b,c,d} J_\eta (\eta_{j,cw}^\dagger \eta_{j,ccw} + \eta_{j,ccw}^\dagger \eta_{j,cw}), \quad (23)$$

is the backscattering-induced interaction terms for the photons transport in different directions.

To realize nonreciprocal band structure, a strong control laser is pumped to the mode $d_{j,cw}$ under the conditions that

the power of the probe laser and the amplitude of acoustic wave are very weak, the modes $d_{j,cw}$ and $d_{j,ccw}$ can be treated classically as complex numbers as

$$\langle d_{j,cw} \rangle = \frac{-i2\Omega_j\kappa_d}{\kappa_d^2 + 4J_d^2} \quad (24)$$

and

$$\langle d_{j,ccw} \rangle = \frac{-i2J_d}{\kappa_d} \langle d_{j,cw} \rangle. \quad (25)$$

So we obtain the linearized Hamiltonian

$$H_{\text{lin}} = H_{1 \rightarrow 3} + H_{3 \rightarrow 1} + H_{\text{BS}}, \quad (26)$$

where

$$H_{1 \rightarrow 3} = \sum_{j=1}^N (g a_{j,cw} c_{j,cw}^\dagger + v a_{j,cw} b_{j,ccw}^\dagger) + \sum_{j=1}^{N-1} v a_{j+1,cw} b_{j,ccw}^\dagger + \text{H.c.}, \quad (27)$$

$$H_{3 \rightarrow 1} = \sum_{j=1}^N (g_s^* a_{j,ccw} c_{j,ccw}^\dagger + v a_{j,ccw} b_{j,cw}^\dagger) + \sum_{j=1}^{N-1} v a_{j+1,ccw} b_{j,cw}^\dagger + \text{H.c.}, \quad (28)$$

and

$$H_{\text{BS}} = \sum_{j=1}^N \sum_{\eta=a,b,c} J_\eta (\eta_{j,cw}^\dagger \eta_{j,ccw} + \eta_{j,ccw}^\dagger \eta_{j,cw}), \quad (29)$$

where $g \equiv g_j \langle d_{j,cw} \rangle$ and $g_s \equiv g_j \langle d_{j,ccw} \rangle$ are the pumping-enhanced photon-phonon coupling strengths; see Fig. 2(b). For simplicity, we set g as a positive-real number. We should point out that g_s is induced by the backscattering as $g_s = (-i2J_d/\kappa_d)g$, and the differences between g and g_s is the key ingredient for the nonreciprocal band structure.

First of all, let us analyze the band structure and the corresponding transmission spectra by neglecting the backscattering, i.e., $g_s = 0$ and $J_\eta = 0$. In this case, the geometric structure of the coupled modes are divided into three parts [see Fig. 2(c)]: (i) a stub lattice [58–60] for the photons transport from Ports 1 to 3, (ii) a Su-Schrieffer-Heeger (SSH) lattice [61–63] for the photons transported from Ports 3 to 1, and (iii) the isolated acoustic modes $c_{j,ccw}$. The Hamiltonian of the stub lattice is given by $H_{1 \rightarrow 3}$ (27), and the SSH lattice and the isolated acoustic modes are described by $H_{3 \rightarrow 1}$ (28) with $g_s = 0$. The band structure of the lattices for photons transported in different directions can be found by numerically solving the eigenvalues of Eqs. (27) and (28), respectively. The band structures for the lattices containing N unit cells ($N = 10$) are shown in Figs. 3(a) and 3(b), respectively. There is only one passband in the band structures of the SSH lattice for photons transport from Ports 3 to 1. In contrast, there are two passbands in the band structures of the stub lattice for the photons transport from Ports 1 to 3, separated by a band gap induced by the photon-phonon interaction g . The width of the band gap becomes broader with the increasing of g , as shown in Fig. 3(c).

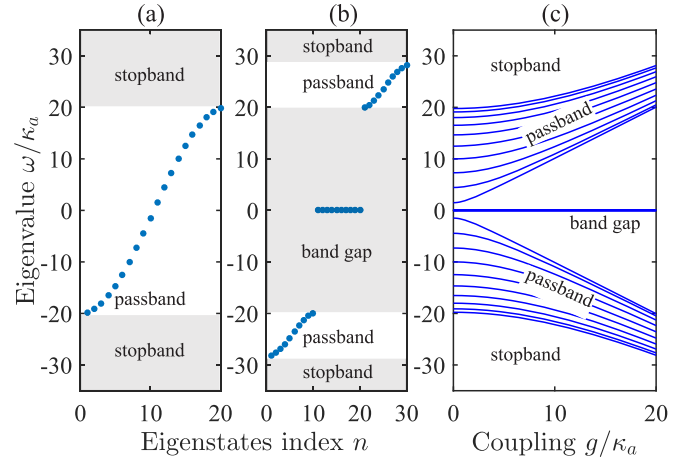


FIG. 3. Band structure of (a) a SSH lattice for the photons transport from Ports 3 to 1 and (b) a stub lattice for the photons transport from Ports 1 to 3. (c) Band structures of the stub lattice versus the coupling strength g/κ_a . The other parameters are $N = 10$, $v = 10\kappa_a$, and $g = 20\kappa_a$ in (b).

The band structures can also be analyzed analytically in the momentum space under the periodic boundary condition. By introducing the Fourier transformation $O_k = (1/\sqrt{N}) \sum_j e^{ijkd_0} O_j$ (k is the wave number and d_0 is the lattice constant, hereafter we set $d_0 = 1$ for simplicity), the Hamiltonian (26) can be rewritten as

$$H_{\text{lin}} = \sum_k V_k^\dagger H_{\text{lin}}(k) V_k, \quad (30)$$

where $V_k^\dagger = (a_{k,cw}^\dagger, b_{k,ccw}^\dagger, c_{k,cw}^\dagger, a_{k,ccw}^\dagger, b_{k,cw}^\dagger, c_{k,ccw}^\dagger)$ and the Hamiltonian in the momentum space is given by

$$H_{\text{lin}}(k) = \begin{pmatrix} H_{1 \rightarrow 3}(k) & H_{\text{BS}}(k) \\ H_{\text{BS}}(k) & H_{3 \rightarrow 1}(k) \end{pmatrix}, \quad (31)$$

with the submatrices

$$H_{1 \rightarrow 3}(k) = \begin{pmatrix} 0 & \rho & g \\ \rho^* & 0 & 0 \\ g & 0 & 0 \end{pmatrix}, \quad (32)$$

$$H_{3 \rightarrow 1}(k) = \begin{pmatrix} 0 & \rho & g_s \\ \rho^* & 0 & 0 \\ g_s^* & 0 & 0 \end{pmatrix}, \quad (33)$$

$$H_{\text{BS}}(k) = \begin{pmatrix} J_a & 0 & 0 \\ 0 & J_b & 0 \\ 0 & 0 & J_c \end{pmatrix}. \quad (34)$$

Here we define $\rho \equiv v + v e^{ik}$.

The frequency spectrum of the lattices can be read off from Eqs. (32) and (33) for $g_s = 0$ and $J_\eta = 0$. The eigenvalues of Eqs. (32) and (33) can be written in an unified form as

$$\omega(k) = \begin{cases} \sqrt{|\rho|^2 + g_{\text{om}}^2}, \\ 0, \\ -\sqrt{|\rho|^2 + g_{\text{om}}^2}, \end{cases} \quad (35)$$

where $g_{\text{om}} = 0$ for the SSH lattice and $g_{\text{om}} = g$ for the stub lattice. As shown in Fig. 4(a), there is only one passband from $-2v$ to $2v$ (width $4v$) in the band structure for the

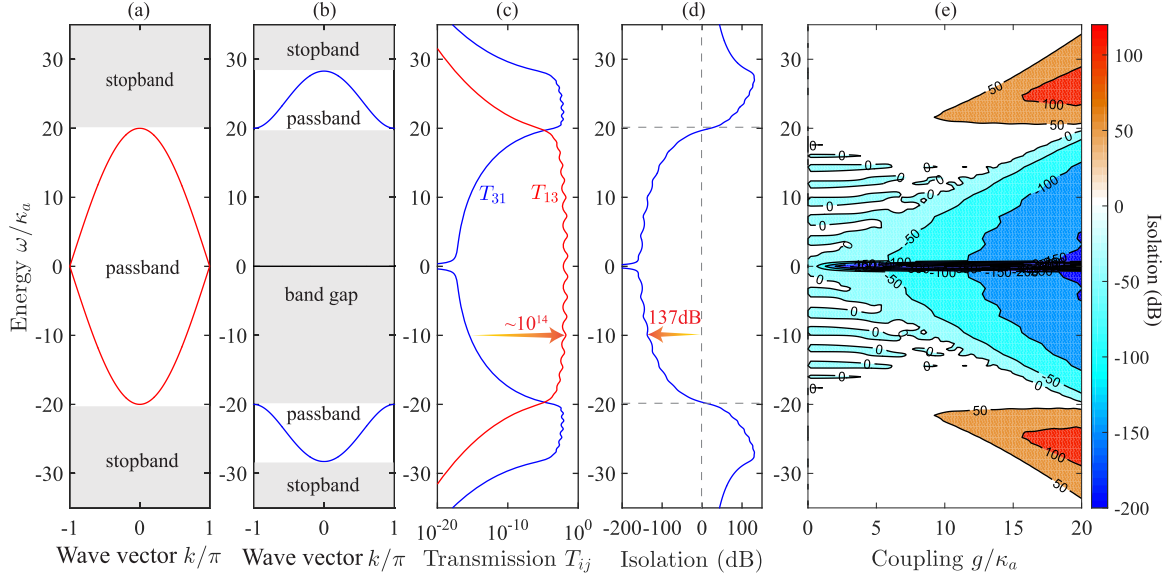


FIG. 4. Frequency spectrum for photons transport (a) from Port 3 to 1 and (b) from Port 1 to 3. (c) The transmission spectra (T_{13} and T_{31}) and (d) the isolation $I = 10 \log_{10}(T_{31}/T_{13})$ versus the energy of the input photons for $N = 10$. (e) The isolation $10 \log_{10}(T_{31}/T_{13})$ versus energy ω/κ_a and coupling strength g/κ_a . The other parameters are $g = 2v$, $v = 10\kappa_a$, $\kappa_a = \kappa_b$, $\kappa_c = \kappa_a/100$, and $J_\eta = 0$ ($\eta = a, b, c, d$).

photons transported from Ports 3 to 1 (SSH lattice), where the eigenvalues $\omega(k) = 0$ for the isolated acoustic modes are not shown here. In contrast, there is a band gap (from g to $-g$) between the two passbands (from g to $\sqrt{4v^2 + g^2}$ and from $-g$ to $-\sqrt{4v^2 + g^2}$) in the band structure of the stub lattice for the photons transport from Ports 1 to 3 [see Fig. 4(b)].

IV. BROADBAND OPTICAL NONRECIPROCALITY

Now, we discuss the transmission spectra between the Ports 1 and 3 with nonreciprocal band structure. After introducing the decay terms and the corresponding input fields, the QLEs for the operators are given by

$$\begin{aligned} \frac{d}{dt}a_{j,cw} &= -ivb_{j,ccw} - ivb_{j-1,ccw} - igc_{j,cw} - iJ_a a_{j,ccw} \\ &\quad - \frac{\kappa_a}{2}a_{j,cw} + \sqrt{\kappa_a}a_{j,cw,in}, \end{aligned} \quad (36)$$

$$\begin{aligned} \frac{d}{dt}b_{j,ccw} &= -iva_{j,cw} - iva_{j+1,cw} - iJ_b b_{j,cw} \\ &\quad - \frac{\kappa_b}{2}b_{j,ccw} + \sqrt{\kappa_b}b_{j,ccw,in}, \end{aligned} \quad (37)$$

$$\begin{aligned} \frac{d}{dt}c_{j,cw} &= -iga_{j,cw} - iJ_c c_{j,ccw} \\ &\quad - \frac{\kappa_c}{2}c_{j,cw} + \sqrt{\kappa_c}c_{j,cw,in}, \end{aligned} \quad (38)$$

$$\begin{aligned} \frac{d}{dt}a_{j,ccw} &= -ivb_{j,cw} - ivb_{j-1,cw} - ig_s c_{j,ccw} - iJ_a a_{j,cw} \\ &\quad - \frac{\kappa_a}{2}a_{j,ccw} + \sqrt{\kappa_a}a_{j,ccw,in}, \end{aligned} \quad (39)$$

$$\begin{aligned} \frac{d}{dt}b_{j,cw} &= -iva_{j,ccw} - iva_{j+1,ccw} - iJ_b b_{j,ccw} \\ &\quad - \frac{\kappa_b}{2}b_{j,cw} + \sqrt{\kappa_b}b_{j,cw,in}, \end{aligned} \quad (40)$$

$$\begin{aligned} \frac{d}{dt}c_{j,ccw} &= -ig_s^* a_{j,ccw} - iJ_c c_{j,cw} \\ &\quad - \frac{\kappa_c}{2}c_{j,ccw} + \sqrt{\kappa_c}c_{j,ccw,in}, \end{aligned} \quad (41)$$

where κ_η ($\eta = a, b, c$) are the decay rate of the optical and mechanical modes, and $\eta_{j,\sigma,in}$ ($\sigma = cw, ccw$) are the input operators of these modes. For the sake of brevity, we rewrite the QLEs in a matrix form as

$$\frac{d}{dt}V = -MV + \sqrt{\Gamma}V_{in}, \quad (42)$$

where $(V)^T = ((V_{1 \rightarrow 3})^T, (V_{3 \rightarrow 1})^T)$, $(V_{1 \rightarrow 3})^T = (\dots, a_{j,cw}, b_{j,ccw}, c_{j,cw}, \dots)$, $(V_{3 \rightarrow 1})^T = (\dots, a_{j,ccw}, b_{j,cw}, c_{j,ccw}, \dots)$, $(V_{in})^T = ((V_{1 \rightarrow 3,in})^T, (V_{3 \rightarrow 1,in})^T)$, $(V_{1 \rightarrow 3,in})^T = (\dots, a_{j,cw,in}, b_{j,ccw,in}, c_{j,cw,in}, \dots)$, $(V_{3 \rightarrow 1,in})^T = (\dots, a_{1,ccw,in}, b_{1,cw,in}, c_{1,ccw,in}, \dots)$, $\Gamma = \text{diag}(\dots, \kappa_a, \kappa_b, \kappa_c, \dots)$, and M is a $6N \times 6N$ coefficient matrix.

We solve the QLEs in the frequency domain and get the expression

$$\tilde{V}(\omega) = (M - i\omega I)^{-1} \sqrt{\Gamma} \tilde{V}_{in}(\omega), \quad (43)$$

where I is the identity matrix. Based on the input-output theory [56], the output vector $(V_{out})^T = ((V_{1 \rightarrow 3,out})^T, (V_{3 \rightarrow 1,out})^T)$, $(V_{1 \rightarrow 3,out})^T = (\dots, a_{j,cw,out}, b_{j,ccw,out}, c_{j,cw,out}, \dots)$, $(V_{3 \rightarrow 1,out})^T = (\dots, a_{1,ccw,out}, b_{1,cw,out}, c_{1,ccw,out}, \dots)$, in the frequency domain is obtained as

$$\tilde{V}_{out}(\omega) = U(\omega) \tilde{V}_{in}(\omega), \quad (44)$$

where

$$U(\omega) = \sqrt{\Gamma}(M - i\omega I)^{-1} \sqrt{\Gamma} - I. \quad (45)$$

The transmission spectrum for the photons transport from Ports 1 to 3 is given by

$$T_{31}(\omega) = |U_{(3N-1),1}(\omega)|^2, \quad (46)$$

and the transmission spectrum in the reverse direction is given by

$$T_{13}(\omega) = |U_{(3N+1),(6N-1)}(\omega)|^2, \quad (47)$$

where $U_{ij}(\omega)$ is the element at the i th row and j th column of the scattering matrix $U(\omega)$ in Eq. (45).

We note that there is a transmission window in the transmission spectrum for the passband, and the photon transport is suppressed significantly in the stopband or band gap. To obtain great optical nonreciprocity, we set $g = 2v$, so the passband ($-2v < \omega < 2v$) for photons transport from Ports 3 to 1 corresponds to the band gap ($-g < \omega < g$) for photons transport from Ports 1 to 3 with two passbands ($-\sqrt{4v^2 + g^2} < \omega < -g$ and $g < \omega < \sqrt{4v^2 + g^2}$), as shown in Figs. 4(a) and 4(b). In this case, the transmission spectra (T_{31} and T_{13}) and the corresponding isolation [$I = 10 \log_{10}(T_{31}/T_{13})$] are shown in Figs. 4(c) and 4(d). We obtain strong nonreciprocity (~ 140 dB) with a broad bandwidth ($\sim g \gg \kappa_a$) based on the nonreciprocal band structure. In addition, the width of the strong nonreciprocity can be tuned by the coupling strength g [see Fig. 4(e)], which depends on the optical driving strength.

To show the advantageous of optical nonreciprocity via the nonreciprocal band structure to the nonreciprocity in the Brillouin optomechanical system with single cavity mode, we show the isolations for different systems in Fig. 5(a) (SC stands for single cavity). In comparison to nonreciprocity in a single cavity, both the isolation and bandwidth are dramatically improved for the nonreciprocity in an optomechanical array with nonreciprocal band structure. Specifically, the isolation is improved by 56 dB for an optomechanical array with $N = 5$ unit cells, and it can be improved further by 72 dB when the unit cells increase to $N = 10$. Moreover, we show the band width with -50 dB isolation versus the number of unit cells N in Fig. 5(b). Clearly, the advantageous of the nonreciprocity in an optomechanical array starts to appear with the number of unit cells $N = 3$, and the bandwidth gradually tends toward $4v$ with the increase of the number of unit cells.

Finally, let us discuss the effect of the backscattering on the nonreciprocity based on nonreciprocal band structure. The backscattering effect induces the coupling between the path for photons transport from Ports 1 to 3 and the path for photons transport from Ports 3 to 1, as shown in Fig. 2(b). In this case, the frequency spectrum versus the wave vector k/π is shown in Fig. 6(a), which is the combination of the energy bands for photons transport in bidirection between Ports 1 and 3. In addition, the backscattering effect induces a nonzero photon-phonon coupling $g_s \neq 0$ for the photons transport from Ports 3 to 1, which leads to the appearing of a band gap $-|g_s| < \omega < |g_s|$ in the band structure. When the backscattering effect is weak, the nonreciprocity still can be obtained with high isolation and broad bandwidth as shown in Figs. 6(b)

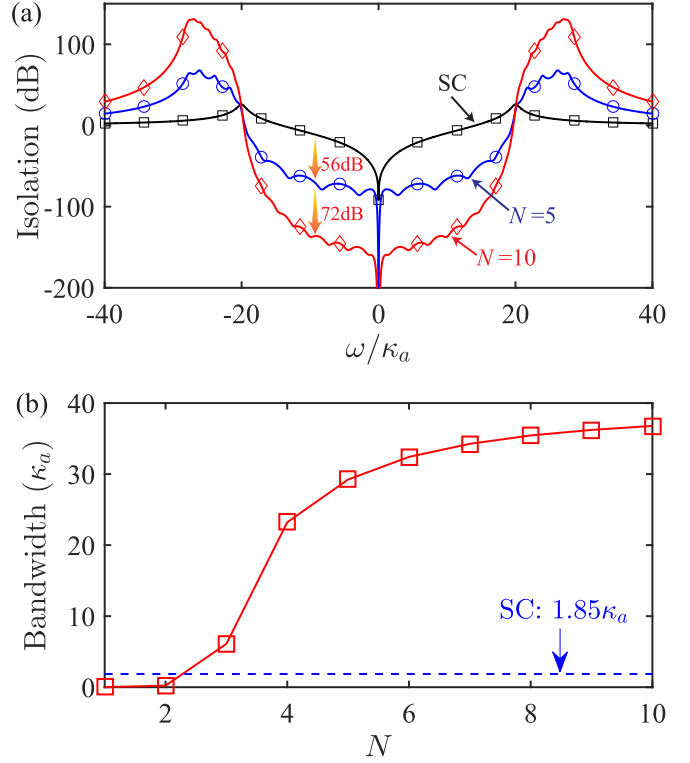


FIG. 5. (a) The isolation $10 \log_{10}(T_{31}/T_{13})$ versus the energy of the input photons ω/κ_a . (b) The bandwidth with isolation of -50 dB versus the number of unit cells N . The dashed line is the bandwidth for optomechanical nonreciprocity in a single cavity. The other parameters are $v = 10\kappa_a$, $g = 2v$, $\kappa_b = \kappa_a$, $\kappa_c = \kappa_a/100$, and $J_\eta = 0$ ($\eta = a, b, c, d$).

and 6(c) for $J_\eta = 0.1\kappa_a$. To show the effect of backscattering on the nonreciprocity clearly, the isolation versus energy ω/κ_a and backscattering J_η/κ_a is shown in Fig. 6(d). We can see that the nonreciprocal effect becomes weaker with the increasing of J_η in the weak backscattering regime ($J_\eta < \kappa_a/2$) and disappears when $J_\eta = \kappa_a/2$. This can be understood from the relation $g_s = (-i2J_d/\kappa_d)g$, which indicates that the difference between g_s and g becomes smaller with the increasing of J_η , and $|g_s| = g$ for $\kappa_d = \kappa_a$ and $J_d = \kappa_d/2$. The permitting transport direction even changes when $J_\eta > \kappa_a/2$ for we have $|g_s| > g$ in the strong backscattering regime. In addition, there are many other factors that may impose some limitation in the isolation contrast, such as the intrinsic decay rates of the coupled optical and acoustic modes, the thermal effect of the acoustic modes, the disorder effect of the parameters, and so on.

V. CONCLUSION

In conclusion, we revealed the challenge in achieving nonreciprocal isolator with both broad bandwidth and high isolation in an optomechanical system with single cavity mode. To overcome this challenge, we proposed a 1D optomechanical array with nonreciprocal band structure to realize broadband optical nonreciprocity. We investigated the nonreciprocal band structure in a 1D Brillouin optome-

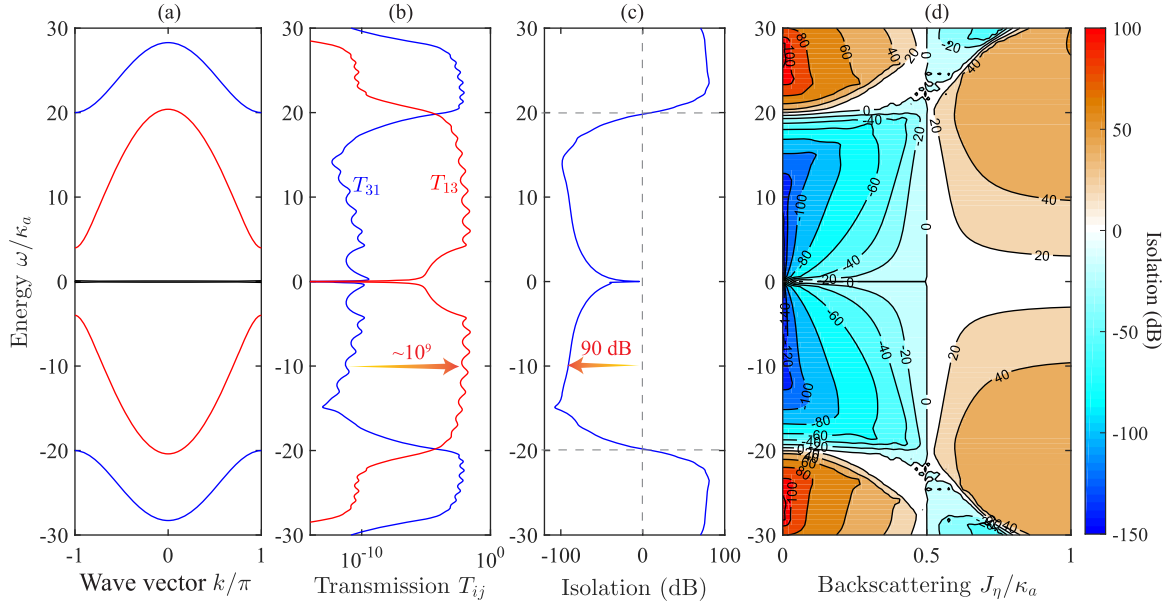


FIG. 6. (a) Frequency spectrum of the Hamiltonian (26) versus wave vector k/π , (b) the transmission spectra (T_{13} and T_{31}), and (c) the isolation $10 \log_{10}(T_{31}/T_{13})$ versus energy ω/κ_a , for $J_\eta = 0.1\kappa_a$ ($\eta = a, b, c, d$). (d) The isolation $10 \log_{10}(T_{31}/T_{13})$ versus energy ω/κ_a and backscattering J_η/κ_a . The other parameters are $v = 10\kappa_a$, $g = 2v$, $\kappa_b = \kappa_d = \kappa_a$, $\kappa_c = \kappa_a/100$, and $N = 10$.

chanical array with directional enhanced optomechanical interaction by applying optical control fields and demonstrated optical nonreciprocity with both broad bandwidth and high isolation in a controllable way. Looking forwards, such optomechanical lattices offer a path to realize proposals exploring the nonreciprocal collective effects, such as nonreciprocal topological phases, and viewed more broadly, it can be used to explore exotic quantum light-matter interactions in nonreciprocal optomechanical lattices [64,65].

ACKNOWLEDGMENTS

This work is supported by the National Natural Science Foundation of China (NSFC) (Grants No. 12064010 and No. 12247105), Natural Science Foundation of Hunan Province of China (Grant No. 2021JJ20036), the science and technology innovation Program of Hunan Province (Grant No. 2022RC1203), and Hunan provincial major sci-tech program (Grant No. 2023ZJ1010), and XL-Lab major project on quantum correlation and quantum network.

- [1] M. Aspelmeyer, T. J. Kippenberg, and F. Marquardt, Cavity optomechanics, *Rev. Mod. Phys.* **86**, 1391 (2014).
- [2] B. P. Abbott *et al.* (LIGO Scientific Collaboration and the Virgo Collaboration), Observation of gravitational waves from a binary black hole merger, *Phys. Rev. Lett.* **116**, 061102 (2016).
- [3] S. Barzanjeh, A. Xuereb, S. Gröblacher, M. Paternostro, C. A. Regal, and E. M. Weig, Optomechanics for quantum technologies, *Nat. Phys.* **18**, 15 (2022).
- [4] E. Verhagen and A. Alù, Optomechanical nonreciprocity, *Nat. Phys.* **13**, 922 (2017).
- [5] S. Manipatruni, J. T. Robinson, and M. Lipson, Optical nonreciprocity in optomechanical structures, *Phys. Rev. Lett.* **102**, 213903 (2009).
- [6] Z. Wang, L. Shi, Y. Liu, X. Xu, and X. Zhang, Optical nonreciprocity in asymmetric optomechanical couplers, *Sci. Rep.* **5**, 8657 (2015).
- [7] X.-W. Xu, L. N. Song, Q. Zheng, Z. H. Wang, and Y. Li, Optomechanically induced nonreciprocity in a three-mode optomechanical system, *Phys. Rev. A* **98**, 063845 (2018).
- [8] L. N. Song, Q. Zheng, X.-W. Xu, C. Jiang, and Y. Li, Optimal unidirectional amplification induced by optical gain in optomechanical systems, *Phys. Rev. A* **100**, 043835 (2019).
- [9] M. Hafezi and P. Rabl, Optomechanically induced nonreciprocity in microring resonators, *Opt. Express* **20**, 7672 (2012).
- [10] B. Li, R. Huang, X. Xu, A. Miranowicz, and H. Jing, Nonreciprocal unconventional photon blockade in a spinning optomechanical system, *Photon. Res.* **7**, 630 (2019).
- [11] X. Xu, Y. Zhao, H. Wang, H. Jing, and A. Chen, Quantum nonreciprocity in quadratic optomechanics, *Photon. Res.* **8**, 143 (2020).
- [12] Z.-X. Tang and X.-W. Xu, Thermal-noise cancellation for optomechanically induced nonreciprocity in a whispering-gallery-mode microresonator, *Phys. Rev. Appl.* **19**, 034093 (2023).
- [13] X.-W. Xu and Y. Li, Optical nonreciprocity and optomechanical circulator in three-mode optomechanical systems, *Phys. Rev. A* **91**, 053854 (2015).
- [14] A. Metelmann and A. A. Clerk, Nonreciprocal photon transmission and amplification via reservoir engineering, *Phys. Rev. X* **5**, 021025 (2015).
- [15] M. Schmidt, S. Kessler, V. Peano, O. Painter, and F. Marquardt, Optomechanical creation of magnetic fields for photons on a lattice, *Optica* **2**, 635 (2015).

- [16] X.-W. Xu, Y. Li, A.-X. Chen, and Y. X. Liu, Nonreciprocal conversion between microwave and optical photons in electro-optomechanical systems, *Phys. Rev. A* **93**, 023827 (2016).
- [17] Y. Li, Y. Y. Huang, X. Z. Zhang, and L. Tian, Optical directional amplification in a three-mode optomechanical system, *Opt. Express* **25**, 18907 (2017).
- [18] L. Tian and Z. Li, Nonreciprocal quantum-state conversion between microwave and optical photons, *Phys. Rev. A* **96**, 013808 (2017).
- [19] C. Jiang, L. N. Song, and Y. Li, Directional amplifier in an optomechanical system with optical gain, *Phys. Rev. A* **97**, 053812 (2018).
- [20] D. Malz, L. D. Tóth, N. R. Bernier, A. K. Feofanov, T. J. Kippenberg, and A. Nunnenkamp, Quantum-limited directional amplifiers with optomechanics, *Phys. Rev. Lett.* **120**, 023601 (2018).
- [21] G. Li, X. Xiao, Y. Li, and X. Wang, Tunable optical nonreciprocity and a phonon-photon router in an optomechanical system with coupled mechanical and optical modes, *Phys. Rev. A* **97**, 023801 (2018).
- [22] Y.-B. Qian, D.-G. Lai, M.-R. Chen, and B.-P. Hou, Nonreciprocal photon transmission with quantum noise reduction via cross-kerr nonlinearity, *Phys. Rev. A* **104**, 033705 (2021).
- [23] A. Seif, W. DeGottardi, K. Esfarjani, and M. Hafezi, Thermal management and non-reciprocal control of phonon flow via optomechanics, *Nat. Commun.* **9**, 1207 (2018).
- [24] S. Barzanjeh, M. Aquilina, and A. Xuereb, Manipulating the flow of thermal noise in quantum devices, *Phys. Rev. Lett.* **120**, 060601 (2018).
- [25] S. J. M. Habraken, K. Stannigel, M. D. Lukin, P. Zoller, and P. Rabl, Continuous mode cooling and phonon routers for phononic quantum networks, *New J. Phys.* **14**, 115004 (2012).
- [26] X.-W. Xu, Y. Li, B. Li, H. Jing, and A.-X. Chen, Nonreciprocity via nonlinearity and synthetic magnetism, *Phys. Rev. Appl.* **13**, 044070 (2020).
- [27] D.-G. Lai, J.-Q. Liao, A. Miranowicz, and F. Nori, Noise-tolerant optomechanical entanglement via synthetic magnetism, *Phys. Rev. Lett.* **129**, 063602 (2022).
- [28] Y.-T. Lan, W.-J. Su, H. Wu, Y. Li, and S.-B. Zheng, Nonreciprocal light transmission via optomechanical parametric interactions, *Opt. Lett.* **47**, 1182 (2022).
- [29] J.-X. Liu, Y.-F. Jiao, Y. Li, X.-W. Xu, Q.-Y. He, and H. Jing, Phase-controlled asymmetric optomechanical entanglement against optical backscattering, *Sci. China Phys. Mech. Astron.* **66**, 230312 (2023).
- [30] J.-Q. Zhang, J.-X. Liu, H.-L. Zhang, Z.-R. Gong, S. Zhang, L.-L. Yan, S.-L. Su, H. Jing, and M. Feng, Topological optomechanical amplifier in synthetic PT-symmetry, *Nanophotonics* **11**, 721 (2022).
- [31] D. Long, X. Mao, G.-Q. Qin, H. Zhang, M. Wang, G.-Q. Li, and G.-L. Long, Dynamical encircling of the exceptional point in a largely detuned multimode optomechanical system, *Phys. Rev. A* **106**, 053515 (2022).
- [32] C.-H. Dong, Z. Shen, C.-L. Zou, Y.-L. Zhang, W. Fu, and G.-C. Guo, Brillouin-scattering-induced transparency and nonreciprocal light storage, *Nat. Commun.* **6**, 6193 (2015).
- [33] J. Kim, M. C. Kuzyk, K. Han, H. Wang, and G. Bahl, Nonreciprocal Brillouin scattering induced transparency, *Nat. Phys.* **11**, 275 (2015).
- [34] Z. Shen, Y.-L. Zhang, Y. Chen, C.-L. Zou, Y.-F. Xiao, X.-B. Zou, F.-W. Sun, G.-C. Guo, and C.-H. Dong, Experimental realization of optomechanically induced non-reciprocity, *Nat. Photon.* **10**, 657 (2016).
- [35] F. Ruesink, M.-A. Miri, A. Alù, and E. Verhagen, Nonreciprocity and magnetic-free isolation based on optomechanical interactions, *Nat. Commun.* **7**, 13662 (2016).
- [36] Z. Shen, Y.-L. Zhang, Y. Chen, F.-W. Sun, X.-B. Zou, G.-C. Guo, C.-L. Zou, and C.-H. Dong, Reconfigurable optomechanical circulator and directional amplifier, *Nat. Commun.* **9**, 1797 (2018).
- [37] F. Ruesink, J. P. Mathew, M.-A. Miri, A. Alù, and E. Verhagen, Optical circulation in a multimode optomechanical resonator, *Nat. Commun.* **9**, 1798 (2018).
- [38] Y. Chen, Y.-L. Zhang, Z. Shen, C.-L. Zou, G.-C. Guo, and C.-H. Dong, Synthetic gauge fields in a single optomechanical resonator, *Phys. Rev. Lett.* **126**, 123603 (2021).
- [39] H. Xu, D. Mason, L. Jiang, and J. G. E. Harris, Topological energy transfer in an optomechanical system with exceptional points, *Nature (London)* **537**, 80 (2016).
- [40] J. Doppler, A. A. Mailybaev, J. Böhm, U. Kuhl, A. Girschik, F. Libisch, T. J. Milburn, P. Rabl, N. Moiseyev, and S. Rotter, Dynamically encircling an exceptional point for asymmetric mode switching, *Nature (London)* **537**, 76 (2016).
- [41] H. Xu, L. Jiang, A. A. Clerk, and J. G. E. Harris, Nonreciprocal control and cooling of phonon modes in an optomechanical system, *Nature (London)* **568**, 65 (2019).
- [42] K. Fang, J. Luo, A. Metelmann, M. H. Matheny, F. Marquardt, A. A. Clerk, and O. Painter, Generalized non-reciprocity in an optomechanical circuit via synthetic magnetism and reservoir engineering, *Nat. Phys.* **13**, 465 (2017).
- [43] J. P. Mathew, J. del Pino, and E. Verhagen, Synthetic gauge fields for phonon transport in a nano-optomechanical system, *Nat. Nanotechnol.* **15**, 198 (2020).
- [44] J. del Pino, J. J. Slim, and E. Verhagen, Non-Hermitian chiral phononics through optomechanically induced squeezing, *Nature (London)* **606**, 82 (2022).
- [45] G. A. Peterson, F. Lecocq, K. Cicak, R. W. Simmonds, J. Aumentado, and J. D. Teufel, Demonstration of efficient nonreciprocity in a microwave optomechanical circuit, *Phys. Rev. X* **7**, 031001 (2017).
- [46] N. R. Bernier, L. D. Tóth, A. Koottandavida, M. A. Ioannou, D. Malz, A. Nunnenkamp, A. K. Feofanov, and T. J. Kippenberg, Nonreciprocal reconfigurable microwave optomechanical circuit, *Nat. Commun.* **8**, 604 (2017).
- [47] S. Barzanjeh, M. Wulf, M. Peruzzo, M. Kalaei, P. B. Dieterle, O. Painter, and J. M. Fink, Mechanical on-chip microwave circulator, *Nat. Commun.* **8**, 953 (2017).
- [48] L. Mercier de Lépinay, E. Damskäg, C. F. Ockeloen-Korppi, and M. A. Sillanpää, Realization of directional amplification in a microwave optomechanical device, *Phys. Rev. Appl.* **11**, 034027 (2019).
- [49] L. M. de Lépinay, C. F. Ockeloen-Korppi, D. Malz, and M. A. Sillanpää, Nonreciprocal transport based on cavity Floquet modes in optomechanics, *Phys. Rev. Lett.* **125**, 023603 (2020).
- [50] J.-S. Tang, W. Nie, L. Tang, M. Chen, X. Su, Y. Lu, F. Nori, and K. Xia, Nonreciprocal single-photon band structure, *Phys. Rev. Lett.* **128**, 203602 (2022).

- [51] H. Ren, T. Shah, H. Pfeifer, C. Brendel, V. Peano, F. Marquardt, and O. Painter, Topological phonon transport in an optomechanical system, *Nat. Commun.* **13**, 3476 (2022).
- [52] A. Youssefi, S. Kono, A. Bancora, M. Chegnizadeh, J. Pan, T. Vovk, and T. J. Kippenberg, Topological lattices realized in superconducting circuit optomechanics, *Nature (London)* **612**, 666 (2022).
- [53] C. Sanavio, V. Peano, and A. Xuereb, Nonreciprocal topological phononics in optomechanical arrays, *Phys. Rev. B* **101**, 085108 (2020).
- [54] M.-A. Lemonde, V. Peano, P. Rabl, and D. G. Angelakis, Quantum state transfer via acoustic edge states in a 2D optomechanical array, *New J. Phys.* **21**, 113030 (2019).
- [55] L. Tang, J. Tang, M. Chen, F. Nori, M. Xiao, and K. Xia, Quantum squeezing induced optical nonreciprocity, *Phys. Rev. Lett.* **128**, 083604 (2022).
- [56] C. W. Gardiner and M. J. Collett, Input and output in damped quantum systems: Quantum stochastic differential equations and the master equation, *Phys. Rev. A* **31**, 3761 (1985).
- [57] M. Zhang, S. Shah, J. Cardenas, and M. Lipson, Synchronization and phase noise reduction in micromechanical oscillator arrays coupled through light, *Phys. Rev. Lett.* **115**, 163902 (2015).
- [58] M. Hyrkäs, V. Apaja, and M. Manninen, Many-particle dynamics of bosons and fermions in quasi-one-dimensional flat-band lattices, *Phys. Rev. A* **87**, 023614 (2013).
- [59] F. Baboux, L. Ge, T. Jacqmin, M. Biondi, E. Galopin, A. Lemaître, L. Le Gratiet, I. Sagnes, S. Schmidt, H. E. Türeci, A. Amo, and J. Bloch, Bosonic condensation and disorder-induced localization in a flat band, *Phys. Rev. Lett.* **116**, 066402 (2016).
- [60] G. Cáceres-Aravena, B. Real, D. Guzmán-Silva, A. Amo, L. E. F. Foa Torres, and R. A. Vicencio, Experimental observation of edge states in SSH-Stub photonic lattices, *Phys. Rev. Res.* **4**, 013185 (2022).
- [61] W. P. Su, J. R. Schrieffer, and A. J. Heeger, Solitons in polyacetylene, *Phys. Rev. Lett.* **42**, 1698 (1979).
- [62] J. K. Asbóth, L. Oroszlány, and A. Pályi, *A Short Course on Topological Insulators: Band-structure Topology and Edge States in One and Two Dimensions* (Springer, Cham, Germany, 2016).
- [63] J. Li, B. Gao, C. Zhu, J. Xu, and Y. Yang, Nonreciprocal photonic composited Su–Schrieffer–Heeger chain, *Appl. Phys. Lett.* **119**, 141108 (2021).
- [64] X.-L. Dong, P.-B. Li, T. Liu, and F. Nori, Unconventional quantum sound-matter interactions in spin-optomechanical-crystal hybrid systems, *Phys. Rev. Lett.* **126**, 203601 (2021).
- [65] X.-L. Dong, P.-B. Li, J.-Q. Chen, F.-L. Li, and F. Nori, Exotic quantum light-matter interactions in bilayer square lattices, *Phys. Rev. B* **108**, 045407 (2023).